Measuring the viscosity of films by thermomechanical analysis: application to metal organic precursor films of functional oxides

Pere Roura-Grabulosa[1] · Jordi Farjas[1] · Joan Pere López-Olmedo[2] · Bohores Villarejo[3] · Susagna Ricart[3] · Xavier Obradors[3] · Teresa Puig[3]

Abstract
We have developed a new method to measure the viscosity of micrometric films by thermomechanical analysis with a hemispherical probe of millimetric diameter. The loading curve (displacement vs. time) recorded as the probe tip crosses the whole film at constant load until it touches the substrate is fitted to a theoretical curve shape that has been obtained after solving the problem of liquid flow under the probe tip. The method has been validated by measuring the viscosity of rosin films. It has been applied to analyze the thermal evolution of unstable liquid films that appear on Ba propionate, Ce(III) propionate and a low-fluorine precursor film of $YBa_2Cu_3O_{6+x}$. During pyrolysis of the last two films, viscosity first diminishes due to heating and then it increases as solid oxide particles are formed inside the liquid.

Keywords Viscosity · Pyrolysis · YBCO · Functional oxides · Thin films · TMA

Introduction

In situ determination of the viscosity of films as a function of temperature is of interest for fundamental questions such as liquid state analysis near the solid–liquid interface [1] and for applied fields such as lubrication [2] or nanoimprint lithography [3, 4]. Likewise, film viscosity monitoring is useful to gain insight into processes such as thermoset crosslinking [4], or to understand the complex interlinked physicochemical transformations that take place during the pyrolysis metal organic precursors [5].

Since the 1980s several techniques have been developed to measure viscosity [1]. Most techniques are based on the response of an arm subjected to a periodic force [3, 7] or the time evolution of the displacement of an indenter [4, 6]. However, contactless methods involving ultrasonic testing [7], the time evolution of deformed nanopatterns under the action of surface tension [8] or the growth rate of a hole during wetting [9] have also been used. Nevertheless, these methods have been applied to stable liquid films or to films whose viscosity has been previously modified by thermal treatments [4]. To our knowledge, none of the published methods have been applied to monitor in situ the viscosity of films whose structure is unstable and evolves with time and temperature.

Thermomechanical analysis (TMA) is well suited to monitor viscosity, because, like any thermoanalytical technique, it is especially designed to control the temperature and the gas atmosphere around the sample. A TMA apparatus measures the change in the linear dimensions of a solid sample when subjected to a given temperature program. Both reversible (thermal expansion) [10] and irreversible variations (dimensional instabilities in plastic parts [11] or shrinking during sintering [12, 13]) can be measured with a coarse control of the load applied to hold the sample. With finer control of the load, a TMA apparatus can be useful to perform creep experiments [14] or to measure viscosity as shown below.

The aim of this work is to present an original method to measure with a TMA apparatus the viscosity of micrometric films deposited on a solid substrate. Its implementation requires minor adaptations of a commercial apparatus, thus

✉ Pere Roura-Grabulosa
 pere.roura@udg.cat

1 GRMT, Department of Physics, University of Girona, Campus Montilivi Edif. PII, 17071 Girona, Catalonia, Spain

2 Unitat d'Anàlisi Tèrmica (STR), University of Girona, Campus Montilivi Edif. PII, 17071 Girona, Catalonia, Spain

3 Institut de Ciència de Materials de Barcelona, ICMAB – CSIC, Campus UA Barcelona, 08193 Bellaterra, Catalonia, Spain

extending the applications of this technique. The method essentially consists of measuring the displacement as a function of time of the TMA probe ("loading curve") during indentation of a liquid film. The probe has a hemispherical tip of radius much larger than film thickness (Fig. 1). Svintsov et al. [4] and Wang et al. [6] applied a similar approach in a nanoindenter. Both used a hemispherical probe (Wang et al. [6] also used a Berkovich probe) and recorded the loading curves. Compared to our technique, they else worked at a different indentation limit (shallow indentation in Wang et al. [6]) or applied loading–unloading cycles (Svintsov et al. [4]). The method by Wang et al. could be applied with a TMA apparatus only in the case of films with very high viscosity ($> 10^{13}$ Pa·s); otherwise the very sharp tip needed to remain in the shallow indentation limit ($d < < H$—Fig. 1a) would imply loads much lower than the minimum load applied by any TMA apparatus. The method by Svintsov et al. will be discussed throughout this article. Neither of the latter two authors performed any test about the accuracy of the measured viscosity values.

The theoretical loading curve is described in Section "The method and its validation." Under reasonable approximations, the solution is analytical, allowing viscosity to be easily quantified by curve fitting. We will show that our method delivers viscosity values of rosin films that are self-consistent when measured under different experimental conditions (applied load, probe radius and film thickness). Furthermore, the absolute value of the viscosity agrees reasonably well with that obtained with an independent technique.
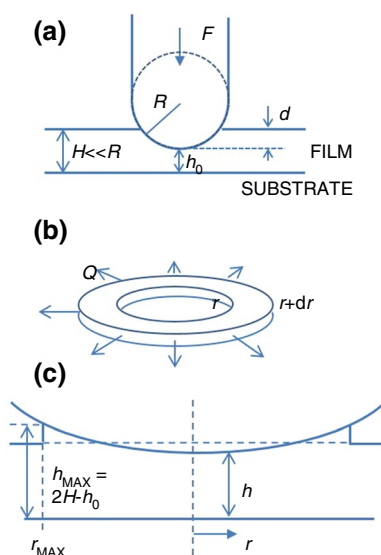
To illustrate the advantages and limitations of our method, it will be applied to measure the evolution of viscosity with temperature of metal organic precursor films for the synthesis of functional oxides (Sections "Thermal evolution of Ce propionate films" "Thermal evolution of a low-fluorine YBCO precursor film"). After deposition, the metal organic films are dried (drying stage) and thermally treated at moderate temperature (pyrolysis stage) to remove the organic ligands, leading to nanometric oxide phases that will react at higher temperature to give rise to the desired crystalline functional phase (crystallization stage) [15, 16]. Loss of the organic mass causes volume shrinkage, which is impeded along the in-plane directions by the substrate. As a result, high stresses arise [17] and, to avoid cracking [18] and wrinkling [19, 20], the film thickness cannot exceed a critical value. Our method was successfully applied to elucidate the mechanism of film wrinkling during pyrolysis and ultimately to grow thicker and defect-free films [5].

The results of Section "Results" will be discussed in Section "Discussion" to foresee the conditions that could lead to liquid formation during thermal processing of metal organic films or similar precursor films, such as those obtained by the sol–gel route or by polymer-assisted deposition. The article ends with a brief summary (Section "Summary").
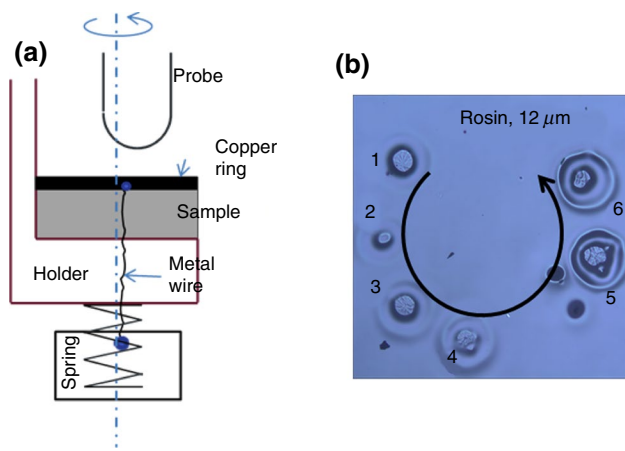
Experimental details

Films preparation

Rosin films about 5 μm thick were prepared by spin-coating on glass substrates (1×1 cm^2) from a solution in ethanol (0.25 g cm^{-3}) at 3000 rpm. They were dried at 80 °C in vacuum. Thicker films required a second deposition. For special experiments, films were sandwiched with a second glass substrate at 120 °C. Optical microscopy revealed bubbles of trapped air with total cross section below 5% of the film area.

Cerium propionate was obtained from Ce(III) acetate according to the procedure detailed in ref. [21]. Ba propionate was obtained from Ba acetate. A solution of 1 g of Ba acetate in 10 mL of propionic acid was heated at 80–90 °C for 20 h. After cooling to room temperature and vacuum distillation of the solvent at 100 °C, Ba propionate was obtained. The product was characterized by NMR. Only signals of Ba propionate were detected.

Ce propionate and Ba propionate films were obtained by drop coating on glass substrates with a micropipette from solutions in propionic acid whose concentration varied depending on the required thickness. The Ce propionate films were dried at room temperature, whereas Ba propionate

Fig. 1 a Geometrical scheme of the system (for convenience, a small hemispherical probe has been drawn, however $H < < R$); **b** radial flow between two parallel discs; c) accumulation of the liquid forming a rim of outer radius r_{MAX}

Fig. 2 a Detail of how the sample is pushed against the holder with the help of a spring. The holder can be manually rotated around its axis, which is eccentric with respect to the probe. b Optical microscopy image showing the footprints produced by the probe on a rosin film after a series of successive tests (rod diameter: 3 mm, size of the image: 2×2 mm.^{2})

films required an extra step at 80 °C in vacuum lasting ½ h to completely evaporate the solvent. After several days, the Ba propionate films became saturated with water.

Finally, $YBa_2Cu_3O_{6+x}$ (YBCO) precursor films were prepared from a solution of $Y(TFA)_3$ (TFA = Trifluoroacetate), Ba acetate and Cu acetate salts dissolved in a mixture of propionic acid (20%) and butanol (80%). The solution was deposited by ink-jet printing on lanthanum aluminum oxide (LAO) substrates and dried at 80 °C (alternative procedures to prepare and deposit similar low-fluorine YBCO precursor films can be found in ref [22].).

TMA and complementary experiments

TMA experiments were carried out with the Setsys Evolution 1700 apparatus of Setaram equipped with fused quartz holder and hemispherical probe of radius 2.5 mm. An additional probe of radius 1.5 mm was homemade from a soda–lime rod. The probes were eccentric with respect to the holder. The samples were fastened at the holder bottom thanks to a metal spring and a copper ring (Fig. 2a). Without this homemade accessory, the recorded displacement was not stable and the liquid films became stuck to the probe impeding to sequentially test several points of the same film during heating. The sample temperature was known from the furnace temperature thanks to previous calibration tests with an extra thermocouple.

Complementary dynamomechanical (DMA) experiments were done with the DMA/SDTA861 apparatus of Mettler Toledo on one rosin film 5 μm thick sandwiched between two glass substrates. During heating at 1 K min^{-1}, the applied load oscillated at 1 Hz.

Finally, the thermal evolution of Ce propionate and Ba propionate films was analyzed by thermogravimetry (TG) and differential scanning calorimetry (DSC) with the TGA/DSC1 and DSC822 apparatus of Mettler Toledo, respectively.

All the experiments were done in a nominally inert atmosphere of N_2.

The method and its validation

Our TMA method for viscosity, η, measurement consists of approaching the probe to the sample at zero load until it touches its surface. Then, a constant positive load, F, is applied pushing the probe tip into the liquid film. The probe velocity, v, diminishes monotonically according to (see Appendix):

$$v \equiv -\frac{dh_0}{dt} = \frac{F}{6\pi\eta R^2} \frac{(2H - h_0)^2 h_0}{4(H - h_0)^2} \quad (1)$$

where H is the film thickness and h_0, the distance between the probe end and the substrate (Fig. 1a). The probe velocity becomes null in contact with the substrate. At this point, to test for any elastic recovery, the load is switched to zero and, finally, a negative load pulls the probe far from the film surface.

During one experiment, the TMA apparatus records the probe displacement as a function of time. If η remains constant, Eq. (1) can be integrated to obtain the loading curve of universal shape:

$$\tau = -\left\{ \frac{2}{2 - \delta} - 2 + \ln\left[(2 - \delta)^3 \cdot \delta\right] \right\} \quad (2)$$

where τ is time, t, normalized to

$$\alpha = \frac{6\pi\eta R^2}{F} \quad (3)$$

and

$$\delta \equiv h_0/H \quad (4)$$

The viscosity of a stable liquid can be determined at discrete temperatures through Eq. (2). Alternatively, if the displacement is measured during a heating ramp, the viscosity dependence on temperature can be obtained through Eq. (1). An intermediate procedure, very useful for the analysis of films that are transformed during heating, consists of testing several points of the film at short temperature intervals without stopping the heating ramp.
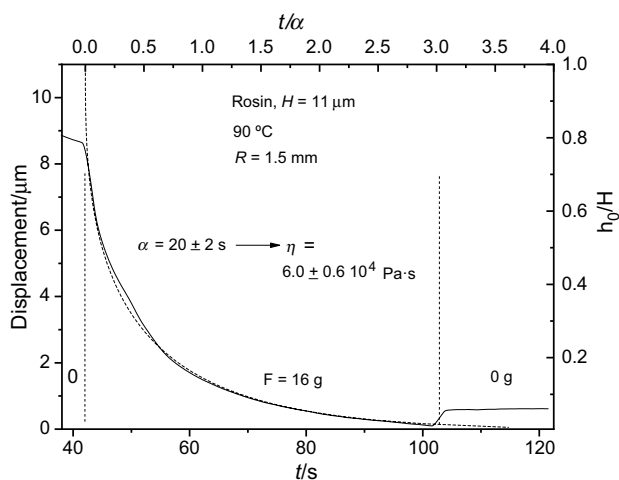
Fig. 3 TMA curve measured on a rosin film at 90ºC (solid line) and the best fit to the theoretical dependence of Eq. (8) (dashed)

Fig. 4 Comparison of the viscosity values of rosin obtained by TMA (squares: R = 2.5 mm, F = 4 g; "x" and circle: R = 1.5 mm, F = 4 g; "+": R = 1.5 mm, F = 16 g) and by DMA. The Voigt mechanical model used for DMA is drawn

If the evolution of η during a single indentation is small, Eq. (2) can be applied.

Thanks to the fact that the probe is eccentric with respect to the holder (Fig. 2a), several points can be analyzed on the film surface by manually rotating the sample holder without need to open the furnace (Fig. 2b). This option is especially important when the film evolves with time or temperature because, between successive measurements, the probe is up and, consequently, any point of the film evolves without the influence of the probe tip. Consequently, a single heating ramp is enough to determine the film evolution with temperature. In contrast, the method of Svintsov et al. [4] requires several loading–unloading cycles on the same point to obtain the viscosity, rendering the influence of the probe on the film evolution more problematic. Our experiments can be performed at isothermal conditions or during a heating ramp.

All the TMA experiments on metal organic films reported in this paper were done during continuous heating. Consequently, measurement of a blank curve without the film was necessary to correct for the displacement of the TMA probe due to differences in thermal expansion between the soda–lime glass probe and the fused silica holder. This blank curve also corrects for the elastic deformation commented below.

To validate the method, the viscosity of rosin films was measured from 80 to 110 °C at isothermal conditions. In Fig. 3, a particular TMA curve obtained from one film 11 μm thick is plotted. The load changes from 0 to 16 g at 42 s. As a consequence of loading, the probe moves down until it reaches the substrate at a vanishing rate. Once the load is removed, the observed elastic recovery is due to the elastic deformation of the substrate holder probe system and not to the film. This parasitic effect can be minimized with
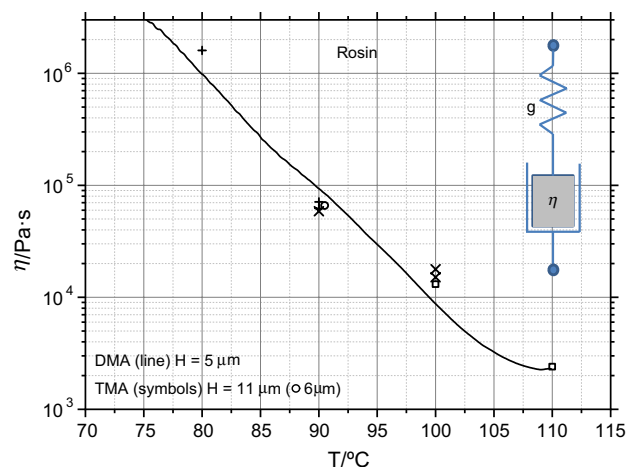
a blank curve measured on an identical substrate without the film. The TMA curve has been satisfactorily fitted to Eq. (2) delivering a value of α (Eq. 3), that corresponds to $\eta = 6.0 \pm 0.6 \cdot 10^4$ Pa·s.

Similar curves were measured on the same film and on a thinner one ($H = 5.9$ μm) with different loads and probe radii to test if the functional dependence on these parameters predicted in Eqs. (3)–(4) is obeyed. As shown in Fig. 4 the viscosity of rosin diminishes by three orders of magnitude when it is heated from 80 to 110 °C. These measurements under different experimental conditions (thickness, applied load and probe radius) leads to a conservative estimation of the error bar of $\Delta\log(\eta) = \pm\log(2)$.

What is left to validate is the absolute value of the measured viscosity. To this aim the viscosity of a rosin film 5 μm thick was measured by the DMA independent technique. A shear oscillating stress was applied to this film sandwiched between two glass substrates (see experimental section). Since the film was indeed liquid, we consider that the external force was applied to a mechanical model consisting of a viscous element (the film) "in series" with an elastic element (the mechanical fixture) of modulus g (Voigt model in Fig. 4) [23] instead of the more usual model "in parallel" (Maxwell model) [23] applied to DMA of solid polymers [24]. From the real (η') and the imaginary (η'') components of the complex viscosity delivered by the DMA apparatus, the η and g values of the model can be calculated:

$$\eta = \frac{\eta''^2}{\eta'} + \eta' \text{ and } \frac{g}{\omega} = \sqrt{\frac{\eta'\eta''}{\eta - \eta'}} \tag{5}$$
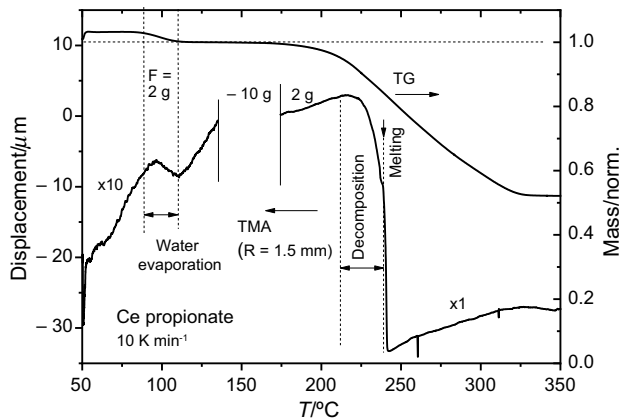
Fig. 5 Mass loss (upper) curve of Ce propionate until complete decomposition into ceria. TMA (lower) curve recording three major processes: water evaporation, initial decomposition and melting

where ω is the frequency of the applied load. The result is plotted in Fig. 4. It agrees fairly well with the values obtained by TMA.

To conclude this section, we can say that the possibility of measuring the viscosity of films by TMA has been validated.

Results

Thermal evolution of Ce propionate films

Ce propionate can be used to obtain ceria thin films and nanoparticles [25, 26], that find applications in fields as diverse as catalysis and electrocatalysis [27], chemical sensors [28], resistive switching devices [29] or as buffer layers for coated superconductor architectures [30].

The evolution of film structure during pyrolysis was analyzed previously [21, 31, 32]. When heated in inert atmosphere, Ce propionate decomposes leaving CeO_2 as solid residue [21]. The three propionate ligands are lost sequentially and substituted by hydroxyl groups, what is revealed by a characteristic signature of several steps in the TG curve measured on Ce propionate powder [21, 26]. In the case of films, a smooth single mass loss step is recorded instead [32]. The process occurs at lower temperature than in powder because of easier out-diffusion of volatiles and the higher reactivity with residual oxygen in films [32]. As expected, the TG curve we measured on one Ce propionate film (Fig. 5) reveals a continuous decomposition process extending from 175 to 325 °C. In addition, the TG curve reveals the evaporation of a small amount of water (3.4 mass%). Since the corresponding step is centered at 100 °C, we deduce that water molecules are not bonded to Ce propionate.

The thermal evolution of Ce propionate films was analyzed by TMA with the aim of detecting the formation of any liquid phase during heating and, in that case, evaluating its viscosity. First, we did an "exploratory experiment" consisting of probing consecutively at a constant load two points of one film during heating. The hemispherical probe remained in contact with the first point from the beginning of the heating ramp until 130 °C. The measured TMA curve has an overall positive displacement of about 2 μm (TMA curve in Fig. 5) due to the difficulty of correcting the differential thermal expansion between the probe and the holder. Despite this parasitic effect, a downward displacement is detected near 100 °C, corresponding to film shrinking due to water evaporation. At 130 °C the probe was lifted several mm from the film, and at 175 °C it was loaded again to a second point on the film to analyze the decomposition step (pyrolysis). At 210 °C a progressive downward displacement begins, revealing film shrinking due to decomposition (TMA curve in Fig. 5). However, although decomposition continues smoothly up to above 300 °C (TG curve), at 235 °C the TMA curve exhibits an abrupt change in the mechanical behavior of the film: The probe reaches the substrate in less than 10 s. The reason is that Ce Propionate melts at this temperature [21, 33], the liquid state being so fluid that the probe moves downward quickly until it reaches the substrate.

We performed a second TMA experiment to quantify the film viscosity during the pyrolysis process. Rotation of the holder allowed us to probe 9 points of the film at temperature intervals of 10 °C between 225 and 310 °C during continuous heating. So, we were able to analyze how viscosity changes as decomposition advances. The TMA curves of this experiment are shown in Fig. 6. Although each curve is identified with a single value of temperature, continuous heating implies that, during the 60 s elapsed
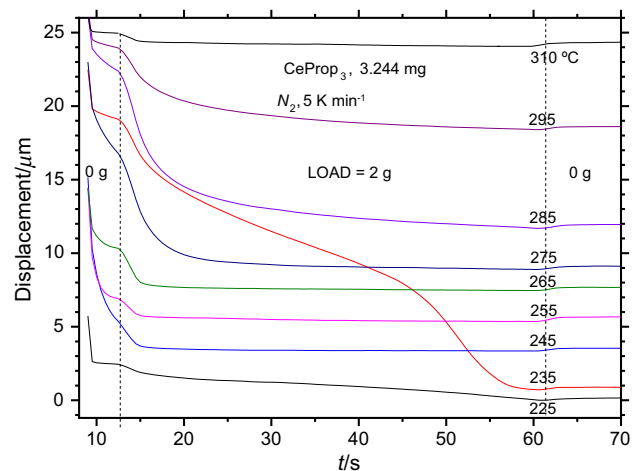

Fig. 6 TMA loading curves of Ce propionate at discrete temperatures (labels are temperatures at the end of the 2 g load)

for each indentation, the sample temperature increased by 5 °C. At low temperature (curve ending at 225 °C), the small displacement indicates that the film is solid; whereas the very large displacement of the 235 °C curve means that, in agreement with the analysis of Fig. 5, melting has occurred in the 230–235 °C interval. So, the transients recorded above 235 °C are related to the film's viscosity. Since the transients become progressively slower from 265 to 295 °C, we conclude that the viscosity increases at higher temperature, in contradiction with the general trend found in all liquids [34]. In fact, the contradiction is only apparent because, during the experiment, higher temperature means a higher decomposition degree and, consequently, a higher amount of solid product embedded in the liquid phase. Quantification of the viscosity below 275 °C has not been possible because the transients are too fast. Fitting the 275 °C curve delivers $\eta = 2 \pm 0.2 \cdot 10^3$ Pa s, whereas we obtain a higher value of $5 \pm 0.5 \cdot 10^3$ Pa s for the 295 °C curve.

Before leaving this subsection, we want to comment on the shape of the curves along the whole loading–unloading sequence and its influence on viscosity quantification. At $t = 7$ s, the load changes from– 10 to 0 g and the probe goes down at a velocity around 200 μm s^{-1} until it touches the film surface (Fig. 6). Since the force needed to displace the liquid tends to zero for $h_0 = H$, probe deceleration at zero load implies a finite indentation in the liquid film before the load of 2 g is applied at $t = 13$ s. This inertial displacement is very large for, say, the 245 °Ccurve where we realize that the probe displacement is still fast just when the 2 g load is applied (Fig. 6). Consequently, the probe displacement during the 2 g load will be always smaller than the film thickness, what adds H as an extra fitting
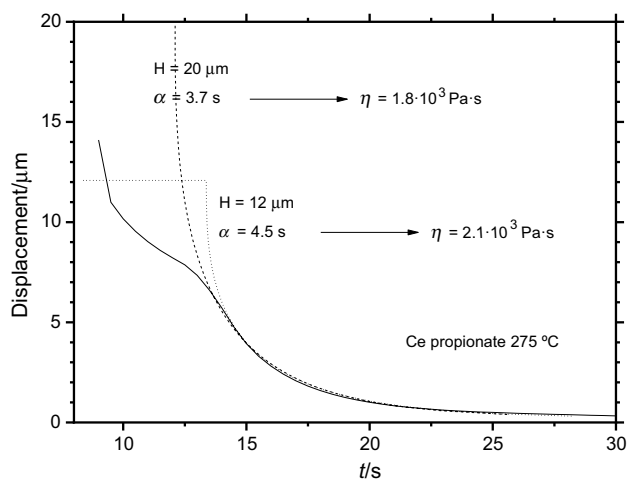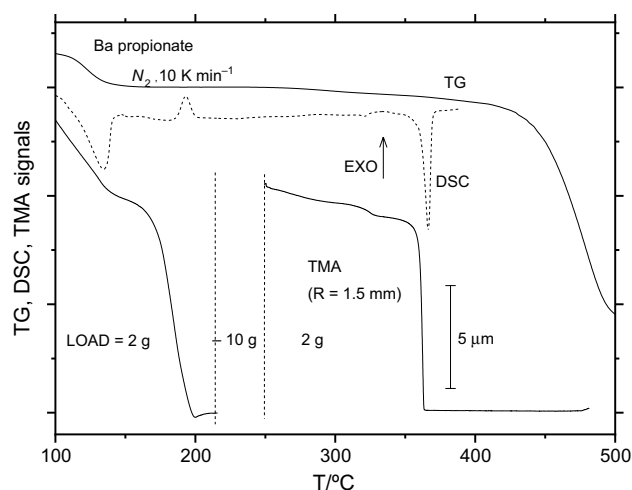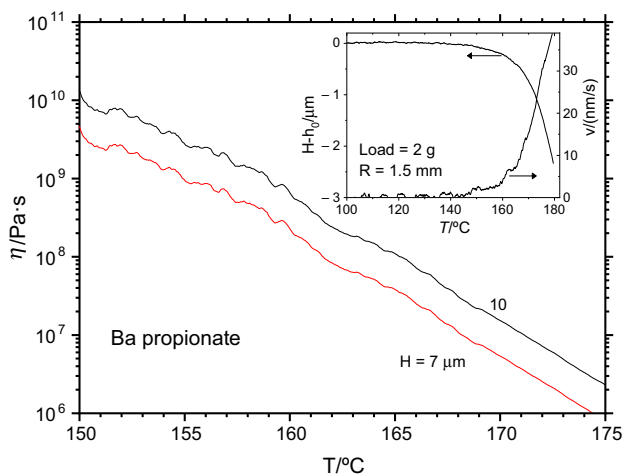

Fig. 8 Mass loss curve (TG) of Ba propionate showing dehydration and decomposition steps. The two endothermic DSC peaks are due to dehydration and melting, whereas the exothermic peak comes from a crystallization process. Just before crystallization, the TMA curve reveals a viscous behavior

parameter. Anyway, taking reasonable values for H results in similar values of η. For instance, at 275 °C we obtain $\eta = 1.8 \cdot 10^3$ and $2.1 \cdot 10^3$ Pa s assuming $H = 20$ and 12 μm, respectively (Fig. 7).

Thermal evolution of Ba propionate films

Ba propionate is a precursor salt that is used in the formulation of solutions, for example, for the synthesis of YBCO superconducting films [22, 35] or BaTiO$_3$ ferroelectric films [18]. Its thermal evolution has been recently studied with the aim of elucidating the decomposition mechanisms of films [36] that differs substantially from those acting in Ba propionate powder [36, 37].

When Ba propionate films are heated in inert atmosphere, the TG curve of Fig. 8 shows a first mass loss step at 120–140 °C due to dehydration. This high "evaporation" temperature (well above 100 °C) is consistent with water molecules incorporated into the crystal structure of hydrated Ba propionate. To elucidate the structure of the dehydration product, the DSC curve is very significant (Fig. 8). After the expected endothermic peak at the dehydration temperature, an exothermic process is detected at 190 °C, which is not related to any mass loss step of the TG curve. The simplest interpretation is that, during dehydration, the film becomes amorphous and crystallizes (an exothermic process) as temperature increases. This phenomenon has been reported for other dehydrated salts. For instance, a high degree of amorphization was reported after dehydration of gadolinium hydrogen phosphate [38], pyrophosphate of potassium and zinc [39] and a complex vanadate [40] (in these papers the mechanical

Fig. 7 TMA curve measured at 275 °C (solid) has been fitted with two different film thicknesses (dotted and dashed) delivering similar values of the viscosity

Fig. 9 Viscosity of the transient liquid obtained after loss of crystallization water in Ba propionate assuming two reasonable values of film thickness. Inset: The experimental TMA curve (left) and its time derivative (right) used to deduce the viscosity

behavior was not tested). TG/DTA curves measured on hydrated Gd propionate are consistent with an (exothermic) crystallization process occurring after dehydration [41]. We have ourselves observed TG/DSC curves similar to those of Fig. 8 for Ce acetate powder. For this particular salt, the amorphous state could be directly assessed because optical micrographs revealed that the dehydration product had flowed like a liquid.

After dehydration, the only mass-loss process detected by TG occurs above 400 °C (Fig. 8), that corresponds to the thermal decomposition of Ba propionate into Ba carbonate.

The TMA curve of Fig. 8 measured with consecutive loading on two points helps to understand the mechanical behavior of the Ba propionate film upon heating. Loading on the first point between room temperature and 210 °C delivers a TMA curve with two steps. The first step, below 140 °C, is related to shrinking due to water-loss. The second, larger, step corresponds to the viscous flow of the amorphous film that becomes more fluid as temperature increases. Loading on the second point above 250 °C results in a very abrupt step in the TMA curve. It begins at the melting point of Ba propionate. Compared to the intermediate TMA step (above 150 °C), the latter is much sharper because the viscosity at this high temperature is much lower.

We tried to measure the viscosity at discrete values of temperature (like in Fig. 6), but we were not able probably because: (a) After dehydration, the temperature range between initial flow and crystallization (from 140 to 180 °C—Fig. 8) is too narrow to allow the measurement of a high viscous liquid; and (b) after melting, at 350 °C, the liquid has a very low viscosity. So, we decided to measure η of the liquid below 200 °C from an experiment at continuous loading. First, we dehydrated the film by heating it

at a 2 K min^{-1} up to 140 °C and cooled it down to obtain an amorphous film. Second, we loaded the probe on this heat-treated film during heating a 10 K min^{-1}. Since, at low temperature, viscosity is very high, the probe did not indent the film resulting in a very horizontal TMA curve below 140 °C, which serves as a good reference to calculate the probe velocity as viscosity diminishes at higher temperature (inset of Fig. 9). Notice that the experiment was stopped at a prove displacement much smaller than the typical thickness of these films (around 8 μm—Fig. 8); i.e., before the probe touched the substrate; consequently, we cannot know the film thickness with accuracy. Application of Eq. (1) with two reasonable values of H, delivers η as a function of temperature. The result is plotted in Fig. 9, where we see that η decreases by 4 orders of magnitude from 150 to 175 °C, where it reaches a value of 0.8–2·10^6 Pa·s.

Thermal evolution of a low-fluorine YBCO precursor film

YBCO is the most widely studied high-temperature superconductor compound [42]. YBCO films have been prepared since the nineties from TFA precursor salts. Although this "TFA-route" has delivered the best YBCO films obtained so far, environmental concern with fluorine has pushed the research toward low-fluorine precursor films [22] like those studied here.

In agreement with a more complete study on the structural evolution of the film [22], present TG experiments have revealed that thermal decomposition of the precursor films ends around 325 °C (Fig. 10) with formation of barium yttrium fluoride and CuO. So, we tested the film's mechanical behavior up to this temperature in steps of 30 °C. The TMA curves
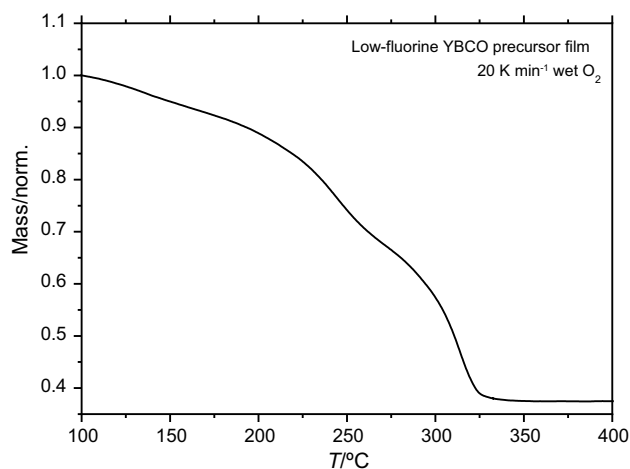
Fig. 10 TG curve of a low-fluorine precursor film of YBCO that would lead to a dense YBCO film 300–400 nm thick after the high-temperature treatment of 800 °C. At 350 °C the precursor film has been transformed into barium yttrium fluoride and CuO [16]
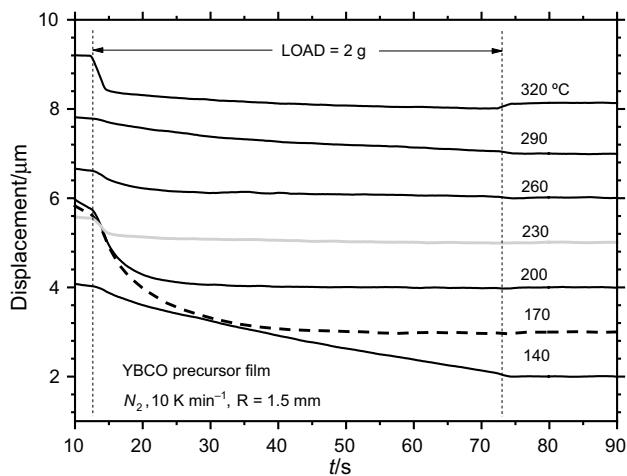
Fig. 11 TMA loading curves of a YBCO precursor film at discrete temperatures (labels are temperatures at the end of the 2 g load)

Fig. 12 Visual evidence of viscous deformation on a YBCO precursor film. The footprint reveals that the material was drawn by the probe tip during unloading (arrows). Even a long fiber crossing the footprint is observed (optical image: 0.3×0.3 mm^2)

measured during a heating ramp are shown in Fig. 11. Except for the curve at 320 °C, which corresponds to an irreversible instantaneous deformation compatible with a fragile behavior, the curves correspond to a liquid film whose viscosity varies with temperature. This liquid behavior reveals the amorphous structure of the as-deposited film. In fact, co-precipitation of the three metal salts during drying impedes crystallization. As a result, the film behaves like a glass (below its glass temperature) or like a gel or a liquid (above it). In this particular case, above 140 °C the film is liquid. In contrast with the other two films, no DSC peaks of melting or crystallization were detected in the YBCO film.

Concerning the dependence of viscosity on temperature, from 140 to 230 °C, the TMA transient becomes faster, i.e., the film's viscosity diminishes. Curve fitting has delivered $\eta = 5.5 \cdot 10^3$ and $2.3 \cdot 10^3$ Pa·s at 170 and 200 °C, respectively. Quantification of η at 140 °C (230 °C) has not been possible because the transient is too slow (fast). Above 230 °C, the evolution goes the other way around; i.e., η diminishes as temperature increases. This behavior would be incomprehensible for an inert liquid. However, the film under study is being transformed onto a solid film due to thermal decomposition. So, we can easily explain the viscosity increment as due to the progressive formation of solid particles embedded in the liquid (as already observed with Ce propionate). Remark that at 290 °C the displacement after 60 s is below 1 μm, whereas it is around 2 μm at 140 °C. Both the mass loss and the partial "solidification" can explain this change.

Direct assessment of viscous deformation has been obtained by optical observation of the footprint left behind by the probe tip (Fig. 12). At the footprint border, the film has been drawn, resulting in the formation of short fibers.
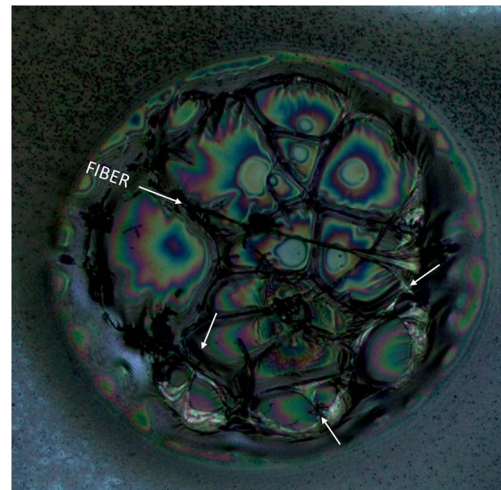
Discussion

Chemical solution deposition of organic precursor salts or the sol–gel process are chemical routes to functional oxide films that need a pyrolysis step to eliminate the organic ligands of the precursor film [43]. The question is whether, during pyrolysis a liquid phase appears similarly to what occurs in polymers [44]. Since a high stress develops as the film shrinks, formation of a liquid phase could be beneficial to relax it, thus avoiding usual defects found on pyrolyzed films such as cracking [18] or wrinkling [5, 19].

To our knowledge, the present paper is the first report devoted to study the rheological behavior of oxide precursor films during pyrolysis, and liquid behavior has been assessed in the three films studied here. The question is, now, "What is the origin of these liquid phases?" The precursor films studied here became liquid due to a process that could be clearly identified: (1) melting of crystalline phases (Ce and Ba propionate melting at 235 and 350 °C, respectively); (2) amorphization during loss of crystallization water in Ba propionate below 140 °C; or (3) co-precipitation of salts in an amorphous structure in the YBCO precursor film.

Probably most pure single metal organic precursors decompose in the solid state unless they melt before or during pyrolysis (up to now, we have found no exception). However, as in the case of the YBCO precursor studied above, "binary" and "ternary" precursors widely used in the preparation of functional oxide films have more chances to reach a liquid state because crystallization after deposition is more difficult and amorphous precursor films become liquid above their glass temperature. Amorphous precursor films can also be obtained when

organic additives (such as TEA, MEA …) are used to control solution rheology or precursor decomposition, and the amorphous state is more easily obtained in the sol–gel route because of the molecular complexity of the precursor [45, 46]. Finally, polymer-assisted deposition always results in amorphous precursor films [47]. This is to say that, although pyrolysis itself does not seem to be the origin of a liquid phase, there may be many instances where pyrolysis occurs when the film is liquid. TMA can help to characterize this unstable liquid.

Compared to the other methods found in the literature to measure the viscosity of films, the use of TMA offers some advantages. First, process temperature control is crucial to define the pyrolysis conditions. This control in ensured in most thermoanalytical techniques as TMA. Concerning the process atmosphere, it must be emphasized that, during pyrolysis, the local atmosphere may differ substantially from the furnace atmosphere [32]. So, with the aim of minimizing the effect of accumulation of volatiles under the probe tip during the decomposition course, the evolution of viscosity is measured discontinuously. In this way, any of the points to be indented remains unperturbed until the beginning of their indentation. Second, the method has been implemented in a commercial apparatus with homemade simple accessories. Presumably, similar adaptations can be implemented in other TMA models.

Our method has also its limitations. First, under the best conditions tested here (isothermal measurements of rosin films), the viscosity is given with an error bar of $\Delta \log(\eta) = \pm \log(2)$. Although this accuracy would be unacceptable for any viscosimeter, one has to take into account that there is no alternative method to measure the evolution of viscosity during film decomposition and that even assessment of liquid behavior may be relevant. Second, the viscosity range that can be measured is about 3 decades wide and centered around 10^4 Pa·s. Lower viscosities could be measured on thinner films with a probe of larger curvature radius, and better control of the probe displacement (particularly with a "softer" impact of the probe on the film's surface before loading) and with control of lower loads. To this aim, implementation of the method with a nanoindenter like that used by Svintsov et al. [4] seems very promising. The viscosity of films can be obtained from the loading curves provided that their behavior is 100% viscous. In case of viscoelastic behavior, the loading curve predicted here is not valid. Although surface tension effects have not been taken into account, deviations from the predicted curve may be significant for low-viscosity films due to wetting of the probe tip.

Summary

It has been shown that the viscosity of liquid films can be measured by TMA. The method consists of recording the displacement vs. time curve (loading curve) of a hemispherical probe when loaded with constant force. Under reasonable simplifications, the loading curve acquires a universal shape when the displacement is normalized to the film's thickness and the time is scaled with a constant proportional to viscosity (Eq. 3). The method has been validated with rosin films 5 and 10 μm thick. Between 80 and 110ºC, their viscosity diminishes by three orders of magnitude and the values obtained by TMA are consistent with those obtained independently by DMA.

The method has been applied to three films of metal organic salts whose structure evolves upon heating, and becomes amorphous with liquid behavior at particular temperature ranges. First, the evolution of liquid Ce propionate during its decomposition into ceria has been analyzed. It has been shown that the film becomes liquid at the melting point of the salt and that, as decomposition progresses, the liquid becomes more viscous due to the highest fraction of solid product embedded in it. Second, we have measured the viscosity of a Ba propionate liquid film after loss of crystallization water and before crystallization of the dehydrated salt. In this case, the TMA loading curve has been recorded during a temperature ramp without unloading the probe. This procedure made it possible to measure continuously the viscosity as a function of temperature. The viscosity decreases by more than four decades from 10^{10} Pa s at 150 °C to 10^6 Pa s at 175 °C. And, finally, it has been shown that a YBCO low-fluorine metal organic precursor film behaves like a liquid above 140 °C. This behavior is due to the film's amorphous structure. It should be noted that the origin of these three particular liquids is not pyrolysis. These three particular films have been chosen to illustrate the technique. It has been argued that presumably many precursor films used in chemical routes to synthesize oxide films (i.e., chemical solution deposition, sol–gel and polymer-assisted deposition) become liquid before or during pyrolysis due to melting of a crystalline phase or softening of an amorphous state.

Appendix: the analytical loading curve

A first sight on the fluid flow under the hemispherical probe (Fig. 1) reveals that, in general, this is a complex problem. Under the probe, the liquid velocity will have an axial component in addition to the radial component

(2D problem). Furthermore, the probe end itself must be described by (r, z) coordinates. On the other hand, the velocity field of the liquid will depend on time (non-steady problem).

Fortunately, the especial conditions of the TMA experiments (micrometric films much thinner than probe radius) allow us to apply several simplifications that lead to an analytical solution for the probe velocity during indentation. First of all, since the liquid flows between two surfaces kept tens of micrometers apart, viscous losses are much higher than pressure variations due to inertia, i.e., the Bernoulli effect can be neglected [48]. In other words, without inertia the state at time t will not depend on the state at time $t-dt$; consequently, the velocity field is that of a steady-state solution consistent with the instantaneous boundary conditions imposed by the probe and the substrate. Second, since the probe radius, R, is much larger than the film thickness, H, beyond a small distance from the axis the radial velocity will be much higher than the axial velocity. So, we will consider a pure radial flow. And, third, $R >> h$ also implies that between r and $r + dr$ the liquid flows between two nearly parallel disks.

The steady radial flow rate Q between two parallel disks separated by h extending from r to $r + dr$ leads to a pressure gradient [48]:

$$\frac{dP}{dr} = -\frac{6\eta}{\pi r h^3} Q(r), \tag{6}$$

where η is viscosity, and volume conservation imposes Q to be equal to the volume swept per unit time by the probe from $r = 0$ to r:

$$Q = \pi r^2 v, \tag{7}$$

where v is the probe velocity. Between r and $r + dr$, P exerts an upward force to the probe equal to:

$$dF = P \cdot 2\pi r dr. \tag{8}$$

So, integration of Eq. (A1) from $r = r_{MAX}$ where $P = 0$ to r delivers $P(r)$ and integration of eq.(A3) from $r = r_{MAX}$ to 0 delivers the force on the probe:

$$F = 6\pi \eta v R^2 \frac{(h_{MAX} - h_0)^2}{h_{MAX}^2 h_0}, \tag{9}$$

where h_0 is the substrate-probe distance and $h_{MAX} = h(r_{MAX})$ (Fig. 1).

An additional assumption has to be made to get closer to the experimental behavior. When the liquid gets out from below the probe, it accumulates there forming a rim, this effect being more pronounced for higher viscosity and probe velocity (the footprints shown in Fig. 2b all contain

these characteristic rims). We assume the simplification that the rim finishes abruptly as sketched in Fig. 1. Volume conservation delivers the value of

$$r_{MAX} = 2\sqrt{R(H - h_0)} \text{ and } h_{MAX} = 2H - h_0, \tag{10}$$

that are exact within the approximation of a parabolic tip ($h << R$). Substitution of Eq. (A5) into Eq. (A4) and rearrangement leads to

$$v \equiv -\frac{dh_0}{dt} = \frac{F}{6\pi \eta R^2} \frac{(2H - h_0)^2 h_0}{4(H - h_0)^2} \tag{11}$$

where F is either the upward force exerted by the liquid on the probe or the constant load that the TMA apparatus applies to the probe. This is so because, along the loading curve, the imbalance due to probe acceleration can be neglected. Experiments have revealed that this condition may not be correct just when the probe enters in contact with the film (see last paragraph of Sect. "- Thermal evolution of Ce propionate films").

If $h_0 = H$ at $t = 0$, and η remains constant during the experiment, integration of Eq. (A6) delivers the predicted TMA loading curve:

$$t = -\alpha \left\{ \frac{2}{2 - h_0/H} - 2 + \ln \left[(2 - h_0/H)^3 \cdot h_0/H \right] \right\}. \tag{12}$$

Svintsov et al. [4] also derived Eq. (A7) but the assumptions leading to this result were not clearly or correctly stated. On the other hand, they applied it to loading–unloading cycles and followed a different analysis procedure to obtain viscosity. We consider that their method gives a qualitative rather than a quantitative evaluation of the viscosity.

Declarations

Conflict of interest The authors have no competing interests to declare that are relevant to the content of this article.

References

1. Israelachvili JN. Measurement of the viscosity of liquids in very thin-films. J Colloid Interf Sci. 1986;100:263–71.
2. Itoh S, Fukuzawa K, Hamamoto Y, Zhang H, Mitsuya Y. Fiber wobbling method for dynamic viscoelastic measurement of liquid lubricant confined in molecularly narrow gaps. Tribol Lett. 2008;30:177–89.
3. Jarzabek DM, Rymuza Z, Horiba A, Hirai Y. Development of an experimental technique for testing rheological properties of ultrathin polymer films used in nanoimprint lithography. J Vac Sci Technol B. 2011;29: 061603.
4. Svintsov AA, Trofimov OV, Zaitsev SI. Viscosity measurement of nanoimprint lithography resists with a rheological nanoindenter. J Vac Sci Technol B. 2007;25:2435–8.
5. Villarejo B, Pop C, Ricart S, Mundet B, Palau A, Roura-Grabulosa P, Farjas J, Puig T, Obradors X. Pyrolysis study of solution-derived superconducting YBa$_2$Cu$_3$O$_7$ films : disentangling the physico-chemical transformations. J Mater Chem C. 2020;8:10266–82.
6. Wang Ch, Liao Y-Ch, Chu J P, Hsueh Ch-H. Viscous flow and viscosity measurement of low-temperature imprintable AuCuSi thin film metallic glasses investigated by nanoindentation creep. Mater Des. 2017;123:112–9.
7. Kasolang S, Dwyer-Joyce RS. Viscosity measurement in thin lubricant films using shear ultrasonic reflection. Proc Inst Mech Eng J J Eng Tribol. 2008;222:423–9.
8. Rognin E, Landis S. Viscosity measurements of thin polymer films from reflow of spatially modulated nanoimprinted patterns. Phys Rev E. 2011;84: 041805.
9. Li CH, Koga T, Jiang J, Sharma S, Narayanan S, Lurio LB, Hu Y, Jiao X, Sinha SK, Billet S, Sosnowik D, Kim H, Sokolov JC, Rafailovic MH. Viscosity measurements of very thin polymer films. Macromolecules. 2005;38:5144–51.
10. Hsueh HB, Chen CY. Preparation and properties of LDHs/epoxy nanocomposites. Polymer. 2003;44:5275–83.
11. Park JK, Kim DS. Effects of an aminosilane and a tetra-functional epoxy on the physical properties of di-functional epoxy/graphene nanoplatelets nanocomposites. Polym Eng Sci. 2014;54:969–76.
12. Greco A, Maffezzoli A. Polymer melting and polymer powder sintering by thermal analysis. J Therm Anal Calorim. 2003;72:1167–74.
13. Sofronia AM, Baies R, Anghel EM, Maritiescu CA, Tanasescu S. Thermal and structural characterization of synthetic and natural nanocrystalline hydroxyapatite. Mater Sci Eng C. 2014;43:153–63.
14. Ahrens M, Lampenscherf S, Vassen R, Stover D. Sintering and creep processes in plasma-sprayed thermal barrier coatings. J Therm Spray Technol. 2004;13:432–42.
15. Lange F. Chemical solution routes to single-crystal thin films. Science. 1996;273:903–9.
16. Schneller T, Waser R, Kosec M, Payne D. Chemical solution deposition of functional oxide films. Berlin: Springer; 2013.
17. Ohno K, Uchiyama H, Kozuka H. Understanding of the development of in-plane residual stress in sol–gel-derived metal oxide thin films. J App Phys. 2012;111: 014901.
18. Kozuka H, Kajimura M. Single-step dip coating of crack-free BaTiO$_3$ films > 1 μm thick: effect of poly(vinylpyrrolidone) on critical thickness. J Am Ceram Soc. 2000;83:1056–62.
19. Zalamova K, Roma N, Pomar A, Morlens S, Puig T, Gazquez J, Carrillo AE, Sandiumenge F, Ricart S, Mestres N, Obradors X. Smooth stress relief of trifluoroacetate metal-organic solutions for YBa$_2$Cu$_3$O$_7$ film growth. Chem Mater. 2006;18:5897–906.
20. Chung JY, Nolte AJ, Stafford CM. Surface wrinkling: a versatile platform for measuring thin-film properties. Adv Mater. 2011;23:349–68.
21. Roura P, Farjas J, Camps J, Ricart S, Arbiol J, Puig T, Obradors X. Decomposition processes and structural transformations of cerium propionate into nanocrystalline ceria at different oxygen partial pressures. J Nanopart Res. 2011;13:4085–96.
22. Palmer X, Pop C, Eloussifi H, Villarejo B, Roura P, Farjas J, Calleja A, Palau A, Obradors X, Puig T, Ricard S. Solution design for low-fluorine trifluoroacetate route to YBa$_2$Cu$_3$O$_7$ films. Supercond Sci Technol. 2016;29: 024002.
23. Christensen RM. Theory of viscoelasticity. London: Academic Press; 1971.
24. Menard KP. Dynamic mechanical analysis. A practical introduction. New York: CRC Press; 1999.
25. Hu J-D, Li Y-X, Zhou X-Z, Cai M-X. Preparation and characterization of ceria nanoparticles using crystalline hydrate cerium propionate as precursor. Mater Lett. 2007;61:4989.
26. Kim M, Hinklin TR, Laine RM. Core-shell nanostructured nanopowders along (CeO$_x$)$_x$(Al$_2$O$_3$)$_{1-x}$ tie-line by liquid-feed flame spray pyrolysis (LF-FSP). Chem Mater. 2008;20:5154.
27. Trovarelli A. Catalytic properties of ceria and CeO$_2$-containing materials. Catal Rev Sci Eng. 1996;38:439–520.
28. Faisal M, Khan SB, Rahman MM, Jamal A, Akhtar K, Abdullah MM. Role of ZnO-CeO$_2$ nanostructures as a photo-catalyst and chemi-sensor. J Mater Sci Technol. 2011;27:594–600.
29. Gonzalez-Rosillo JC, Ortega-Hernandez R, Arndt B, Coll M, Dittmann R, Obradors X, Palau A, Suñe J, Puig T. Engineering oxygen migration for homogeneous volume resistive switching in 3-terminal devices. Adv Electron Mater. 2019;5:1800629.
30. Goyal A, Parans PM, Schoop U. The RABiTS approach: using rolling-assisted biaxially textured substrates for high-performance YBCO superconductors. MRS Bull. 2004;29:552–61.
31. Roura P, Farjas J, Ricart S, Aklalouch M, Guzman R, Arbiol J, Puig T, Calleja A, Peña-Rodríguez O, Garriga M, Obradors X. Synthesis of nanocrystalline ceria thin films by low-temperature thermal decomposition of Ce-propionate. Thin Solid Films. 2012;520:1949–53.
32. Roura P, Farjas J, Eloussifi H, Carreras L, Ricart S, Puig T, Obradors X. Thermal analysis of metal organic precursors for functional oxide preparation: thin films versus powders. Thermochim Acta. 2015;601:1–8.
33. Ogawa M, Manabe K. Formation of dilanthanide monooxide tetrapropionate by thermal-decomposition of propionate monohydrate of rare-earth elements (La, Ce, Pr, Nd). Nippon Nagaku Kaishi. 1993;5:617–22.

34. Bird RB, Stewart WE, Lightfoot EN. Transport phenomena. 2nd ed. New York: John Wiley & Sons Inc; 2007.

35. Soler L, Jareño J, Banchewski J, Rasi S, Chamorro N, Guzman R, Yáñez R, Mocuta C, Ricart S, Farjas J, Roura-Grabulosa P, Obradors X, Puig T. Ultrafast transient liquid assisted growth of high current density superconducting films. Nat Commun. 2020;11:344.

36. Rasi S, Ricart S, Obradors X, Puig T, Roura-Grabulosa P, Farjas J. Radical and oxidative pathways in the pyrolysis of a barium propionate-acetate salt. J Anal Appl Pyrol. 2019;141: 104640.

37. Gobert-Ranchoux E, Charbonnier F. Comportement thermique des propionates hydrates de calcium, strontium et barium. J Therm Anal. 1977;12:33–42.

38. Chehimi-Moumen F, Llewellyn P, Rouquerol F, Vacquier G, Ben Hassen-Chehimi D, Ferid M, Trabelsi-Ayadi M. Constant transformation rate thermal analysis of $HGdP_2O_7 \cdot 3H_2O$. J Therm Anal Calorim. 2005;82:783–9.

39. Ciopec M, Muntean C, Negrea A, Lupa L, Negrea P, Barvinschi P. Synthesis and thermal behavior of double copper and potassium pyrophosphate. Thermochim Acta. 2009;488:10–6.

40. de Fernandez Luis R, Urtiaga MK, Mesa JL, Larrea ES, Iglesias M, Rojo T, Arriortua MI. Thermal response, catalytic activity, and color change of the first hybrid vanadate containing BPE guest molecules. Inorg Chem. 2013;52:2615–26.

41. Grivel J-C. Thermal decomposition of $RE(C_2H_5CO_2)_3 \cdot H_2O$ (RE = Dy, Tb, Gd, Eu and Sm). J Therm Anal Calorim. 2014;115:1253–64.

42. Shiohara Y, Taneda T, Yoshizumi M. Overview of materials and power applications of coated conductors project. Jpn J Appl Phys. 2012;51(1R): 010007.

43. Schwartz R, Schneller T, Waser R. Chemical solution deposition of electronic oxide films. CR Chimie. 2004;7:433–61.

44. Uddin MA, Koizumi K, Murata K, Sakata Y. Thermal and catalytic degradation of structurally different types of polyethylene into fuel oil. Polym Degrad Stabil. 1997;56:37–44.

45. Attia SM, Wang J, Wu GM, Shen J, Ma JH. Review on sol-gel derived coatings: process, techniques and optical applications. J Mater Sci Technol. 2002;18:211–8.

46. Zaharescu M, Predoana L, Pandele J. Relevance of thermal analysis for sol–gel-derived nanomaterials. J Sol–Gel Sci Technol. 2018;86:7–23.

47. Jia QX, McCleskey TM, Burrell AK, Lin Y, Collis GE, Wang H, Li ADQ, Foltyn SR. Polymer-assisted deposition of metal-oxide films. Nat Mater. 2004;3:529–32.

48. Armengol J, Calbo J, Pujol J, Roura P. Bernoulli correction to viscous losses: radial flow between two parallel discs. Am J Phys. 2008;76:730–7.